




Tailoring the superposition of finite-momentum valley exciton states in transition-metal dichalcogenide monolayers by using polarized twisted light

Guan-Hao Peng, Oscar Javier Gomez Sanchez , Wei-Hua Li, Ping-Yuan Lo , and Shun-Jen Cheng *

Department of Electrophysics, National Yang Ming Chiao Tung University, Hsinchu 300, Taiwan



(Received 24 February 2022; revised 23 September 2022; accepted 29 September 2022; published 11 October 2022)

A twisted light is a spatially structured light that carries quantized orbital angular momenta (OAM), being a new degree of freedom useful in quantum information technology in addition to that of intrinsic spin angular momentum (SAM), i.e., polarization. Using polarized twisted light to excite valley excitons in transition-metal dichalcogenide monolayers (TMD-ML's) sets up an intriguing photoexcited system which couples comprehensively the excitonic and photonic multi-degrees of freedom, including the center-of-mass motion and valley polarization of exciton and the both optical OAM and SAM. In this work, we present a systematic theoretical investigation of the photoexcited valley excitons in TMD-ML's by polarized Laguerre-Gaussian beams, one of the best known twisted light (TL). We show that the photoexcitation of polarized TL incident to a TMD-ML leads to the formation of the superposition of finite-momentum exciton (SFME) states, spatially localized with the OAM- and SAM-encoded geometrical patterns.

DOI: [10.1103/PhysRevB.106.155304](https://doi.org/10.1103/PhysRevB.106.155304)

I. INTRODUCTION

With the intriguing electronic and excitonic properties, atomically thin transition-metal dichalcogenide monolayers (TMD-ML's) have drawn vast attention for over a decade and been well realized nowadays as promising two-dimensional (2D) materials for advanced optoelectronic and valley-based photonic applications [1–4]. Because of inherently weak Coulomb screening in the 2D structures, photogenerated electron-hole (e - h) pairs in a TMD-ML form tightly bound excitons via the enhanced Coulomb attractions, with the exciton binding energy so high as hundreds of meV [5,6]. It is such tightly bound excitons, rather than the free e - h pairs, that dictate the major optical features of the atomically thin 2D materials and various extraordinary optical and excitonic phenomena result in the 2D materials, e.g., room-temperature formation of exciton-polariton [7,8], high-temperature exciton condensation [9], ultrafast excitation energy transfer [10,11], superiorly high efficiencies of luminescences [1] and light harvest [12,13], and rich exciton fine structures [14–24].

Even more interestingly, an exciton in a TMD-ML possesses multiple degrees of freedom, including spin, valley, and center-of-mass momentum (\mathcal{Q}) as well. The spin-valley locking effect in D_{3h} TMD-ML's enables the selective photogeneration of exciton in specific K or K' valley and the coherent manipulation of the superposition valley exciton states by using the polarization of light, i.e., optical spin angular momentum (SAM), of the incident light. This sets up the prospect of valley-based photonics and quantum technology implemented on TMD-ML's [2,3]. By contrast to the maturity of the manipulation of the spin-valley-locked degrees of

freedom, manipulating the center-of-mass (CoM) motion of exciton yet remains as a nontrivial task because the charge neutrality of exciton hinders the electrically bias-controlled transport or confinement [25–27].

The conventional light sources used for the photogeneration of excitons are commonly based on nonstructured laser beams that carry the optical SAM only. In fact, a light can be spatially structured to acquire additional degrees of freedom, e.g., optical orbital angular momentum (OAM). Such structured light with quantized OAM, also referred to as twisted light (TL), was first predicted by Allen *et al.* in the early 90s [28] and soon later realized experimentally by He *et al.* [29]. Over the past three decades, such new states of photons have inspired broad interest and persistently on-going progress in the exploration of the fascinating optical physics and the advanced OAM-based photonic technology [30,31], such as multidimensional quantum entanglements [32], OAM-encoded quantum communications [33,34], optical control of microscopic systems [35,36], and high-resolution imaging [37]. Following the state-of-the-art advancement in the technology of TL, it is timely crucial to study the light-matter interactions between TL and optoelectronic materials for the prospective development of TL-based optoelectronic systems. However, the research on the photoexcitation of TL in solids, especially the emergent 2D materials, are yet still very limited [38,39].

The first observation of the interaction between TL and TMD-ML's was reported very recently by Ref. [40], with our theoretical contributions. Following the pioneering experiment-theory-joint work, in this paper we for the first time present a comprehensive theoretical investigation of the photoexcited valley excitons in TMD-ML's by polarized Laguerre-Gaussian beams, one of the best known TL carrying the optical angular momenta, both OAM and SAM. We show that the photoexcitations of TL lead to the formation

*Corresponding author: sjcheng@nycu.edu.tw

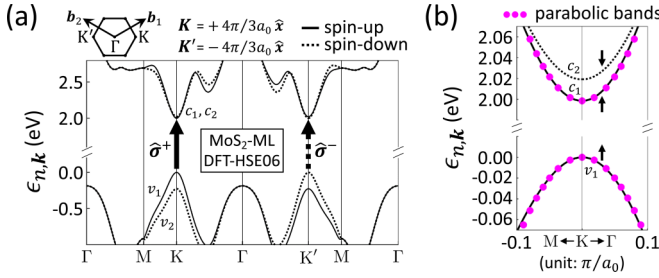


FIG. 1. (a) The DFT-calculated spin- and valley-characteristic quasiparticle band structure of MoS₂-ML. (b) The zoom-in band dispersion of the lowest conduction ($\epsilon_{c_1,k}$) and topmost valence bands ($\epsilon_{v_1,k}$) around the K valley, which can be well fitted by the ideally parabolic bands (magenta dots) with effective mass $m_c = 0.39m_0$ and $m_v = 0.46m_0$, respectively. For MoS₂-ML, the bright A-exciton states involve mainly the spin-like v_1 and the c_1 bands.

of superposition of finite-momentum exciton (SFME) states in TMD-ML's [41], constituted by the OAM- and SAM-dependent superposition of the exciton states with different CoM momenta. Via the couplings between optical angular momenta and the momentum-dependent transition dipoles of valley exciton, those TL-induced SFME states in TMD-ML's are featured with the momentum-dependent optical matrix elements as the manifestation of the intriguing interplay between the multiple degrees of freedom of valley exciton and TL, including both optical SAM and OAM.

This article is organized as follows. Following the introductory section, Section II systematically presents the fundamental theories of valley excitons in 2D materials and Laguerre-Gaussian TL, the light-matter interactions between 2D excitons and TL, and the photoexcitation of excitons by TL. We begin with the pseudospin model of exciton for the bright exciton states with small CoM momenta in MoS₂-ML's with the fitted parameters, which are determined on the first principles base. In the valley-exciton model, we present the theory of exciton-light interaction between the valley exciton states of MoS₂-ML and the Laguerre-Gaussian TL in the angular spectrum representation. Taking the time-dependent perturbation theory, we derive the formalism for the TL-induced formation of SFME states and simulate the \mathbf{q} -dependent optical matrix elements of the resulting SFME states with respect to the plane wave of light with the wave vector \mathbf{q} . Section III presents and analyzes the calculated results, including the photoexcitation of SFME states by TL with controlled OAM and SAM, and the OAM- and SAM-encoded shape geometries and optical matrix elements of TL-generated SFME states. Section IV concludes this work.

II. THEORY

A. Valley-characteristic band structures of TMD-ML's

The band structure of a TMD-ML is characterized by two distinctive valleys located at the K and K' corners of the first Brillouin zone (BZ), where the conduction and valence bands are separated by the direct band gaps in the visible light regime. Figure 1(a) presents the spin-resolved quasiparticle band structure, $\epsilon_{n,k}$, of a MoS₂ monolayer calculated by using the first-principles VASP package [42]

in the density-functional-theory (DFT) with the use of Heyd-Scuseria-Ernzerhof (HSE) functional model (see Ref. [43] for details) [44–47]. Because of the strong spin-orbit couplings (SOCs) in TMD-ML's, the conduction (valence) bands, $\epsilon_{c,k}$ ($\epsilon_{v,k}$), in the valleys are spin split by Δ_c (Δ_v) in the scale of tens (hundreds) of meV. The giant spin-splitting in the valence band spectrally separates apart the two classes of exciton states, i.e., the A exciton (B exciton) in the low (high) energy regime. The meV-scaled spin-splitting Δ_c further lifts the degeneracy of the spin-allowed bright states and the spin-forbidden dark ones in the excitonic fine structure of A-exciton. Throughout this work, we shall focus on the low-lying spin-allowed A-exciton states of MoS₂-ML that involve mainly the topmost valence band and lowest spinlike conduction band around the K and K' valleys. Figure 1(b) shows the DFT-calculated dispersions of the lowest conduction and the topmost valence band around the K valley of MoS₂-ML, well fitted by the parabolic conduction and valence bands with the effective masses, $m_c = 0.39m_0$ and $m_v = 0.46m_0$, respectively, where m_0 is the electron rest mass.

B. Valley excitons in TMD-ML's

In this section, we present the exciton pseudospin model [21,23,50] for the bright exciton states, $|\Psi_{S,\mathbf{Q}}^X\rangle \equiv \frac{1}{\sqrt{\Omega}} \sum_{vck} \Lambda_{S,\mathbf{Q}}(vck) \hat{c}_{c,k+\mathbf{Q}}^\dagger \hat{h}_{v,-k}^\dagger |GS\rangle$, with small CoM momenta, \mathbf{Q} , in MoS₂-ML's, which is used for the studies of TMD-ML's under TL excitation throughout this work. The exciton model is parametrized by the exciton mass, binding energy and e - h exchange interaction that are determined on the first principles base (see Ref. [43] for technical details) [21,23,24,40,51,52]. S is the band index, Ω is the total area of the 2D material, $\hat{c}_{c,k}^\dagger$ ($\hat{h}_{v,-k}^\dagger$) is the particle operator that creates a conduction electron (valence hole) in the Bloch state $\psi_{c,k}(\mathbf{r})$ ($\psi_{v,k}(\mathbf{r})$), $|GS\rangle$ is the ground state with fully occupied valence bands, and $\Lambda_{S,\mathbf{Q}}(vck)$ is the amplitude of the e - h configuration $\hat{c}_{c,k+\mathbf{Q}}^\dagger \hat{h}_{v,-k}^\dagger |GS\rangle$.

Taking the exchange-free exciton doublet with the well-specified valley character as basis, $|\Psi_{\tau=K/K'}^{X(0)}\rangle = \frac{1}{\sqrt{\Omega}} \sum_{vck} \Lambda_{\tau=K/K'}^{(0)}(vck) \hat{c}_{c,k+\mathbf{Q}}^\dagger \hat{h}_{v,-k}^\dagger |GS\rangle$, the exciton Hamiltonian can be expressed in the form of 2×2 matrix, as given by [21,23,50], which reads

$$\hat{H}_X(\mathbf{Q}) = \begin{pmatrix} E_{K,\mathbf{Q}}^{X(0)} + \tilde{\Delta}_{K,K}(\mathbf{Q}) & \tilde{\Delta}_{K,K'}(\mathbf{Q}) \\ \tilde{\Delta}_{K,K'}^*(\mathbf{Q}) & E_{K',\mathbf{Q}}^{X(0)} + \tilde{\Delta}_{K',K'}(\mathbf{Q}) \end{pmatrix} + E_{\text{SR}}^X I_{2 \times 2}, \quad (1)$$

where $E_{\tau,\mathbf{Q}}^{X(0)} = (E_g - 4Ry^X) + \hbar^2|\mathbf{Q}|^2/2M_X$ is the energy dispersion of exchange-free exciton, E_g is the energy gap, Ry^X is the Rydberg constant of exciton, $M_X = m_c + m_v = 0.85m_0$ is the total effective mass of exciton, $\Lambda_{\tau,\mathbf{Q}}^{(0)}(vck)$ is the momentum-space wave function of the exchange-free lowest 1s exciton states that could be derived from the Wannier equation, [51,53–56] the superscript (0) is used to indicate the exchange-free nature and the label of exciton state is changed to $S \rightarrow \tau = K/K'$ to specify the valley of exciton, and $\tilde{\Delta}_{\tau,\tau'}(\mathbf{Q})$ are the matrix elements of the long-range (LR) e - h exchange Coulomb interaction (see Ref. [43] for details).

The second term on the right-handed side of Eq. (1) arises from the short-range (SR) part of e - h exchange Coulomb interaction and simply shifts upward the bright exciton doublet by the constant energy, E_{SR}^X , from the lowest level of the exchange-irrelevant spin-forbidden dark exciton states. Since the energy offset of short-range exchange interaction essentially does not affect the bright-exciton band structure, hereafter we disregard E_{SR}^X (set to be zero) for brevity. Considering that bright exciton states lying in the small reciprocal area of light cone and expanding the periodic part of the Bloch function as $u_{n,\mathbf{k}+\mathbf{Q}}(\mathbf{r}) \approx u_{n,\mathbf{k}}(\mathbf{r}) + \mathbf{Q} \cdot \nabla_{\mathbf{k}} u_{n,\mathbf{k}}(\mathbf{r})$, [21,23,50] the matrix element of the LR e - h exchange Coulomb interaction [57,58] is approximated to

$$\tilde{\Delta}_{\tau,\tau}(\mathbf{Q}) \approx \frac{1}{\Omega} \frac{1}{2\epsilon_0 Q} (\mathbf{Q} \cdot \mathbf{D}_{\tau,\mathbf{Q}}^{X*}) (\mathbf{Q} \cdot \mathbf{D}_{\tau,\mathbf{Q}}^X), \quad (2)$$

in terms of the transition dipole moment of exciton $\mathbf{D}_{\tau,\mathbf{Q}}^X \equiv \frac{1}{\sqrt{\Omega}} \sum_{vck} \Lambda_{\tau,vck}^{(0)} (vck) \mathbf{d}_{v,k;c,k}$, where $\mathbf{d}_{v,k;c,k} \equiv e \langle \psi_{v,k} | \mathbf{r} | \psi_{c,k} \rangle = \frac{e\hbar}{im_0(\epsilon_{v,k} - \epsilon_{c,k})} \langle \psi_{v,k} | \mathbf{p} | \psi_{c,k} \rangle$ is the single-particle transition dipole moment. [23,50] In small \mathbf{Q} -limit, the dipole moments of valley excitons have the approximated form of $\mathbf{D}_{K/K',\mathbf{Q}}^X = D_0^X \hat{\sigma}^{\pm}$, where $\hat{\sigma}^{\pm} = \frac{1}{\sqrt{2}} (\hat{x} \pm i\hat{y})$. From the DFT-calculated band structure and the DFT-based Bethe-Salpeter equation (BSE) calculation [23,59,60], we obtain $D_0^X/\sqrt{\Omega} = 0.181|e|$ (see Ref. [43] for details). The explicit form of Eq. (2) in small \mathbf{Q} limit is expressed as $\tilde{\Delta}_{K,K}(\mathbf{Q}) = \tilde{\Delta}_{K',K'}(\mathbf{Q}) = \gamma|\mathbf{Q}|$ and $\tilde{\Delta}_{K,K'}(\mathbf{Q}) = \tilde{\Delta}_{K',K}^*(\mathbf{Q}) = \gamma|\mathbf{Q}|e^{-i2\phi_{\mathbf{Q}}}$, where $\gamma \equiv (1/4\epsilon_0)(D_0^X/\sqrt{\Omega})^2$ is the strength factor of the e - h exchange interaction, and $\phi_{\mathbf{Q}} \equiv \tan^{-1}(Q_y/Q_x)$ is the azimuthal angle of \mathbf{Q} .

By diagonalizing Eq. (1), the valley-mixed exciton states are solved as

$$|\Psi_{\pm,\mathbf{Q}}^X\rangle = \frac{1}{\sqrt{2}} (e^{-i\phi_{\mathbf{Q}}} |\Psi_{K,\mathbf{Q}}^{X(0)}\rangle \pm e^{i\phi_{\mathbf{Q}}} |\Psi_{K',\mathbf{Q}}^{X(0)}\rangle), \quad (3)$$

with the eigenenergies

$$E_{\pm,\mathbf{Q}}^X = E_{\tau,\mathbf{Q}}^{X(0)} + (1 \pm 1)\gamma|\mathbf{Q}|, \quad (4)$$

which are split by the \mathbf{Q} -dependent exchange interaction into the linear upper band $E_{+,\mathbf{Q}}^X$ and the parabolic lower band $E_{-,\mathbf{Q}}^X$, respectively. The slope of the linear upper band is evaluated as $2\gamma = \frac{1}{2\epsilon_0} (\frac{D_0^X}{\sqrt{\Omega}})^2 \approx 2.94 \text{ eV \AA}$ from the DFT-calculated $D_0^X/\sqrt{\Omega}$ [40], leading to the exciton band splitting $\sim 2.8 \text{ meV}$ at the light-cone edge [see Fig. 2(d)]. In this work, we adopt the choice of phases in Ref. [21] to fix the global phases of the valley-mixed exciton states in Eq. (3). Following Eq. (3), the transition dipole moment of the exciton eigenstate with the momentum \mathbf{Q} in the upper band is given by

$$\mathbf{D}_{+,\mathbf{Q}}^X = \frac{1}{\sqrt{2}} (e^{-i\phi_{\mathbf{Q}}} \mathbf{D}_{K,\mathbf{Q}}^X + e^{i\phi_{\mathbf{Q}}} \mathbf{D}_{K',\mathbf{Q}}^X) = D_0^X(\mathbf{Q}/|\mathbf{Q}|) \quad (5)$$

and that of the exciton state with the same momentum in the lower band is

$$\mathbf{D}_{-,\mathbf{Q}}^X = \frac{1}{\sqrt{2}} (e^{-i\phi_{\mathbf{Q}}} \mathbf{D}_{K,\mathbf{Q}}^X - e^{i\phi_{\mathbf{Q}}} \mathbf{D}_{K',\mathbf{Q}}^X) = iD_0^X(\mathbf{Q}_{\perp}/|\mathbf{Q}|), \quad (6)$$

where $\mathbf{Q}_{\perp} \equiv |\mathbf{Q}|(-\sin\phi_{\mathbf{Q}}\hat{x} + \cos\phi_{\mathbf{Q}}\hat{y})$ is perpendicular to \mathbf{Q} . One notes that the exciton dipole moment of upper (lower)

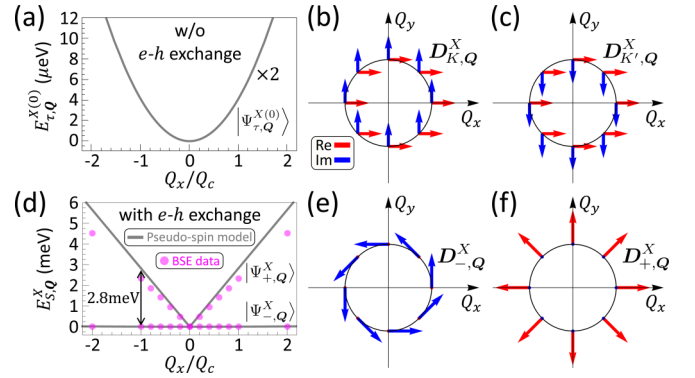


FIG. 2. (a) The lowest valley degenerate exciton bands of MoS₂-ML, regardless of e - h exchange interaction, along the Q_x axis around the light-cone reciprocal range, where $\mathbf{Q} = (Q_x, Q_y)$ is the wave vector of exciton and the band edge is offset to be zero. (b) The complex transition dipole moments of the K -valley exciton states and (c) those of the K' -valley exciton states over the \mathbf{Q} -space. The red (blue) arrows denote the real (imaginary) parts of the excitonic dipole moments. In the absence of e - h exchange interaction, the dipole moments of the K - and K' -valley exciton states follow the opposite circular polarization, independent of \mathbf{Q} . (d) The valley-split exciton bands by e - h exchange interaction of MoS₂-ML, calculated by numerically solving the DFT-based Bethe-Salpeter equation (magenta circles) and simulated by the parametrized pseudospin model (gray curves). The e - h exchange interaction splits the degenerate exciton bands into the linear upper band ($S = +$) and the parabolic lower one ($S = -$), leading to the \mathbf{Q} -dependent dipole moments of the exciton states, $\mathbf{D}_{S,\mathbf{Q}}^X$. (e) The \mathbf{Q} -dependent transition dipole moments, $\mathbf{D}_{-,\mathbf{Q}}^X$, of the lower exciton band are shown to be transverse with respect to the \mathbf{Q} wave vector, while (f) the dipole moments, $\mathbf{D}_{+,\mathbf{Q}}^X$, of the upper exciton band states are longitudinal. One notes that all the \mathbf{Q} vectors shown here are normalized by the light-cone radius $Q_c = (1.92 \text{ eV})/\hbar c$, where 1.92 eV is the measured energy of A-exciton peak in the absorption spectra of MoS₂-ML [48,49].

exciton band is longitudinal (transverse) with respect to the exciton wave vector, i.e., $\mathbf{D}_{+,\mathbf{Q}}^X \parallel \mathbf{Q}$ ($\mathbf{D}_{-,\mathbf{Q}}^X \perp \mathbf{Q}$).

Figure 2(d) presents the calculated valley-mixed bright exciton bands split by the e - h exchange interaction in the \mathbf{Q} space covering the light-cone area by using Eq. (4) with the parameter $\gamma = 1.47 \text{ eV \AA}$, in agreement with the band structures calculated by solving the BSE (see Ref. [43] for technical details) [40]. Correspondingly, the transition dipole moments of the valley-mixed exciton states with finite \mathbf{Q} in the lower and upper bands are plotted in Figs. 2(e) and 2(f), respectively. Figures 2(e) and 2(f) show that the dipole moments of the valley-mixed excitons are \mathbf{Q} -dependent, where $\mathbf{D}_{+/-,\mathbf{Q}}^X$ of the upper longitudinal/lower transverse band is always pointing to the direction parallel/normal to \mathbf{Q} . For comparison, Figures 2(a)–2(c) show the calculated valley-degenerate parabolic exciton bands and the exciton dipole moments in circular polarization of bright valley exciton without the consideration of e - h exchange interaction. The choice of phases in Eq. (3) is advantageous for the simple expression of the dipole moment of the valley-mixed exciton states in Eqs. (5) and (6), which are expressed as purely real and imaginary \mathbf{Q} -dependent vectors, respectively. This makes the \mathbf{Q} -dependent dipole moments straightforwardly to visualize [see Figs. 2(e)

and 2(f)] and facilitate the later analysis on the exciton-light interactions.

C. Twisted light: Laguerre-Gaussian beams

Throughout this work, we consider the twisted light in the Laguerre-Gaussian (LG) modes characterized with the quantized orbital angular momentum (OAM) $\ell = 0, \pm 1, \pm 2, \dots$ and radial mode index $p = 0, 1, 2, \dots$ that are normally incident on TMD-ML's [28]. Experimentally, LG beams with the well-controlled OAMs can be realized by using the technology of spatial light modulator (SLM), and have been employed to photoexcite atoms [61], molecules [62,63], and free electrons in crystals [64], but not extensively yet excitons in solids [38–40]. In the angular spectrum representation (see Ref. [43] for details), the vector potential of the LG beam in Lorenz gauge under the long Rayleigh-length condition [65] and the paraxial approximation (that is valid for not too large ℓ) can be decomposed in the 2D Fourier transform [66,67] as

$$\mathbf{A}_{q_0}^{\hat{\mathbf{e}}, \ell, p}(\mathbf{r}) = \hat{\mathbf{e}} \sum_{q_{\parallel}} \mathcal{A}_{\ell p}(q_{\parallel}) e^{iq \cdot \mathbf{r}}, \quad (7)$$

where $\mathbf{q} = \mathbf{q}_{\parallel} + \mathbf{q}_0$, $\mathbf{q}_{\parallel} = q_x \hat{\mathbf{x}} + q_y \hat{\mathbf{y}}$, $\mathbf{q}_0 = q_0 \hat{\mathbf{z}}$ is the wave vector specified to be along the direction of light propagation, and $\hat{\mathbf{e}}$ denotes the unit vector of polarization perpendicular to \mathbf{q}_0 . As derived by Ref. [40] the \mathbf{q}_{\parallel} -space amplitude function of LG beam (see Figs. S2 and S3 in Ref. [43]) is given by

$$\mathcal{A}_{\ell p}(q_{\parallel}) = \tilde{F}_{\ell p}(q_{\parallel}) e^{i\ell \phi_{q_{\parallel}}}, \quad (8)$$

in terms of the complex-valued radial function $\tilde{F}_{\ell p}(q_{\parallel}) = e^{-i\ell\pi/2} e^{i\eta\pi} F_{\ell p}(q_{\parallel})$ and the phase factor $e^{i\ell \phi_{q_{\parallel}}}$, where $q_{\parallel} = \sqrt{q_x^2 + q_y^2}$, $\phi_{q_{\parallel}} = \tan^{-1}(q_y/q_x)$, $\eta_{\ell} \equiv |\ell| [1 - \Theta(\ell)]$, $\Theta(\ell)$ is the Heaviside function, and $F_{\ell p}(q_{\parallel}) = (2\pi A_0^{\text{LG}}/\Omega) \mathcal{H}_{|\ell|}[f_{\ell p}(\rho)]$ is the real-valued radial function obtained by means of the Hankel transform $\mathcal{H}_{|\ell|}[f_{\ell p}(\rho)] = \int_0^{\infty} d\rho \rho f_{\ell p}(\rho) J_{|\ell|}(q_{\parallel}\rho)$ of order $|\ell|$ with $J_{|\ell|}(q_{\parallel}\rho)$ being the Bessel function of the first kind of order $|\ell|$ [67].

Taking the form of Eq. (7), a TL can be viewed as a superposition of a large number of the plane waves with distinct wave vectors $\mathbf{q} = (\mathbf{q}_{\parallel}, q_0)$, each of which propagates with the amplitude of $\mathcal{A}_{\ell p}(q_{\parallel})$ in the slightly different directions inclined from that of \mathbf{q}_0 with the angles, $\theta = \tan^{-1}(|\mathbf{q}_{\parallel}|/|q_0|)$, depending on \mathbf{q}_{\parallel} ($\theta \ll 1$ in the paraxial approximation). As shown later, the amplitude $\mathcal{A}_{\ell p}(q_{\parallel})$ determines the magnitude of optical matrix element with which the finite-momentum exciton state with $\mathbf{Q} = \mathbf{q}_{\parallel} \neq \mathbf{0}$ can be photoexcited by TL. In the limit of small θ , it is shown by Ref. [68] that the formalism of LG beam formulated in Lorenz gauge can be approximated by that of the same beam in the Coulomb gauge. Under the condition, one can incorporate the formalism of Eq. (7) for the TL in the paraxial approximation into the light-matter interaction theory presented in the next section which is set up on the base of Coulomb gauge [36].

D. Exciton-light interaction

In this section, we present the formalisms for the exciton-light interaction between 2D valley exciton and LG TL

formulated in the angular spectrum representation. Taking the rotating wave approximation, one writes the light-matter interaction induced by a weak TL as $H_I(\mathbf{r}, t) \approx \tilde{H}_I(\mathbf{r}) e^{-i\omega t}$, where $\tilde{H}_I(\mathbf{r}) = \frac{|e|}{2m_0} \mathbf{A}(\mathbf{r}) \cdot \mathbf{p}$.

In the time-dependent perturbation theory, the time-dependent exciton state under a weak photoexcitation can be expressed as

$$|\Psi^X(t)\rangle \approx |GS\rangle + \sum_{S=\pm} \sum_{\mathbf{Q}} \tilde{c}_{S,\mathbf{Q}}^{(1)}(t) e^{-i\omega_S \mathbf{Q} t} |\Psi_{S,\mathbf{Q}}^X\rangle, \quad (9)$$

a superposition of finite-momentum exciton (SFME) state, where $\tilde{c}_{S,\mathbf{Q}}^{(1)}(t)$ are the TL-induced time-dependent coefficients of the photogenerated exciton states, $|\Psi_{S,\mathbf{Q}}^X\rangle$. In the first-order perturbation theory, one solves $\tilde{c}_{S,\mathbf{Q}}^{(1)}(t) = \tilde{\gamma}_{S,\mathbf{Q}}(t) (\frac{\tilde{M}_{S,\mathbf{Q}}}{\hbar \omega_{S,\mathbf{Q}}})$, where $\tilde{\gamma}_{S,\mathbf{Q}}(t)$ absorbs the all time dependence of the coefficient, $\tilde{M}_{S,\mathbf{Q}} = \frac{1}{\sqrt{\Omega}} \sum_{vck} \Lambda_{S,\mathbf{Q}}^*(vck) \langle \psi_{c,k+\mathbf{Q}} | \frac{|e|}{2m_0} \mathbf{A}(\mathbf{r}) \cdot \mathbf{p} | \psi_{v,k} \rangle$ is the optical matrix element that measures the optical activity of the exciton state $|\Psi_{S,\mathbf{Q}}^X\rangle$ with respect to the incident light, ω is the light frequency, and $\omega_{S,\mathbf{Q}} = E_{S,\mathbf{Q}}^X/\hbar$ is the natural frequency of the exciton state $|\Psi_{S,\mathbf{Q}}^X\rangle$.

For normally incident nonstructured light, the vector potentials are generally given by $\mathbf{A}_{q_0}^{\hat{\mathbf{e}}}(\mathbf{r}) = \hat{\mathbf{e}} A_0 e^{iq_0 \cdot \mathbf{r}}$, specified by a well-defined wave vector \mathbf{q}_0 . Taking the vector potential of plane-wave light for $\tilde{M}_{S,\mathbf{Q}}$, the optical matrix element of the exciton state $|\Psi_{S,\mathbf{Q}}^X\rangle$ in the electric dipole approximation is derived as $\tilde{M}_{S,\mathbf{Q}}^{\hat{\mathbf{e}}, q_0} \approx \delta_{\mathbf{Q}, \mathbf{0}} (E_g/2i\hbar) A_0 (\hat{\mathbf{e}} \cdot \mathbf{D}_{S,\mathbf{Q}}^{X*})$, where the Kronecker delta, $\delta_{\mathbf{Q}, \mathbf{0}}$, ensuring the conservation of momentum allows only the exciton state with vanishing $\mathbf{Q} = \mathbf{0}$ coupled to the normal incident light with $\mathbf{q}_{\parallel} = \mathbf{0}$.

By contrast, a TL is composed of infinite number of finite-momentum plane waves and the optical matrix element in terms of the vector potential of TL, $\mathbf{A}_{q_0}^{\hat{\mathbf{e}}, \ell, p}(\mathbf{r}) = \hat{\mathbf{e}} \sum_{q_{\parallel}} \mathcal{A}_{\ell p}(q_{\parallel}) e^{iq \cdot \mathbf{r}}$ according to Eq. (7), is written as $\tilde{M}_{S,\mathbf{Q}}^{\hat{\mathbf{e}}, \ell, p} = \frac{1}{\sqrt{\Omega}} \sum_{vck} \Lambda_{S,\mathbf{Q}}^*(vck) \sum_{q_{\parallel}} \frac{|e|}{2m_0} \mathcal{A}_{\ell p}(q_{\parallel}) \hat{\mathbf{e}} \cdot \langle \psi_{c,k+\mathbf{Q}} | e^{iq \cdot \mathbf{r}} \mathbf{p} | \psi_{v,k} \rangle$. In the electrical dipole approximation, one can preserve the leading electrical dipole term in the Taylor expansion of the Bloch state $\psi_{c,k+\mathbf{Q}}$ around \mathbf{k} and approximate $\langle \psi_{c,k+\mathbf{Q}} | e^{iq \cdot \mathbf{r}} \mathbf{p} | \psi_{v,k} \rangle \approx \delta_{q_{\parallel}, \mathbf{Q}} \langle \psi_{c,k} | \mathbf{p} | \psi_{v,k} \rangle$ in the evaluation of the optical matrix element, where the in-plane momenta \mathbf{q}_{\parallel} carried by TL enter the delta function to ensure the momentum conservation $\mathbf{q}_{\parallel} = \mathbf{Q}$. As a result, the optical matrix element of the exciton state $|\Psi_{S,\mathbf{Q}}^X\rangle$ is derived as

$$\tilde{M}_{S,\mathbf{Q}}^{\hat{\mathbf{e}}, \ell, p} \approx \left(\frac{E_g}{2i\hbar} \right) \mathcal{A}_{\ell p}(\mathbf{Q}) (\hat{\mathbf{e}} \cdot \mathbf{D}_{S,\mathbf{Q}}^{X*}). \quad (10)$$

in terms of the exciton dipole, $\mathbf{D}_{S,\mathbf{Q}}^X$, defined for Eq. (2).

The \mathbf{Q} -dependent optical matrix element of Eq. (10) is determined by the product of the OAM-determined spectrum distribution function of LG beam, $\mathcal{A}_{\ell p}(\mathbf{Q})$, over the extended \mathbf{Q} -space and the projection of exciton transition dipole moment on the polarization direction, $(\hat{\mathbf{e}} \cdot \mathbf{D}_{S,\mathbf{Q}}^{X*})$, i.e., the coupling between the optical SAM, $\hat{\mathbf{e}}$, of TL and the valley-mixed transition dipole of exciton by the intrinsic e - h exchange interaction. The magnitude of the optical matrix element evaluated by Eq. (10) reflects the coupling strength for the exciton-light interaction between a valley exciton in

the state (S, \mathbf{Q}) and a $\hat{\mathbf{e}}$ -polarized TL in the (ℓ, p) mode, manifesting the intriguing couplings between the multiple degrees of freedom possessed by the optical and excitonic subsystems. With the \mathbf{Q} -dependent nonzero optical matrix elements given by Eq. (10), a LG beam enables the simultaneous photogeneration of numerous distinct finite-moment exciton states, $|\Psi_{S,\mathbf{Q}}^X\rangle$, forming a SFME state.

E. TL induced SFME states

To characterize the spatial localization of a SFME state, here we introduce the envelope function of SFME state in the center-of-mass coordinates \mathbf{R}_c defined by

$$\tilde{F}_S(\mathbf{R}_c, t) = \frac{1}{\sqrt{\Omega}} \sum_{\mathbf{Q}} \tilde{c}_{S,\mathbf{Q}}^{(1)}(t) e^{i\mathbf{Q}\cdot\mathbf{R}_c}, \quad (11)$$

which extracts the \mathbf{R}_c -coordinate envelope profile from the exciton wave function given by Eq. (9). To elaborate on the dynamics of SFME states, we consider the energy dispersions, $E_{\pm,\mathbf{Q}}^X$, of valley exciton bands, which are described by $E_{-\mathbf{Q}}^X = \hbar^2|\mathbf{Q}|^2/2M_X$ and $E_{+\mathbf{Q}}^X \approx 2\gamma|\mathbf{Q}|$ for the lower and upper bands, respectively (the band edge is offset to be zero here). It is known that $\tilde{F}_S(\mathbf{R}_c, t)$ as a superposition of the finite momentum exciton states of the S band formed by momentum states around a wave vector \mathbf{Q} moves with the group velocity defined by $\mathbf{v}_{S=\pm,\mathbf{Q}} \equiv (\nabla_{\mathbf{Q}} E_{\pm,\mathbf{Q}}^X)/\hbar$, according to which $v_{-,\mathbf{Q}} = \hbar|\mathbf{Q}|/M_X$ and $v_{+,\mathbf{Q}} = 2\gamma/\hbar$ are derived. Since an SFME state induced by a twisted light is composed of the momentum exciton states with various \mathbf{Q} , each of which are oriented in all possible in-plane directions. Thus one might expect that, with increasing time, the envelope function of the TL-induced SFME state might be unmoving but spread more and more extendedly over the in-plane space with the group velocity. With the parameters $\gamma = 1.47$ eV Å and $M_X = 0.85m_0$, $v_{-,\mathbf{Q}}$ ($v_{+,\mathbf{Q}}$) at the major momentum $|\mathbf{Q}| = 0.1Q_c$ of SFME state of Figs. 5(c)–5(e) is estimated to be 1.33×10^{11} nm/s (4.46×10^{14} nm/s). Thus one could infer that, within the measured decoherence time ~ 0.4 ps by Ref. [69], the envelope function of the SFME states of the upper band could quickly be flattened over the space while the envelope function of the lower band SFME states might remain more stable in the geometric shape. The phase velocity of $\tilde{F}_S(\mathbf{R}_c, t)$ is given by $\mathbf{v}_{S=\pm,\mathbf{Q}} \equiv (E_{\pm,\mathbf{Q}}^X/\hbar|\mathbf{Q}|)\hat{\mathbf{Q}}$, which has the magnitude of $v_{-,\mathbf{Q}} = \hbar|\mathbf{Q}|/2M_X = v_{-,\mathbf{g}}/2$ and $v_{+,\mathbf{Q}} = 2\gamma/\hbar = v_{+,\mathbf{g}}$.

Neglecting the slight phase interference between the time-dependent parts ($\propto e^{-i\omega_S \mathbf{Q}t}$) of the different exciton states and considering $\omega_{S,\mathbf{Q}} \approx \omega_0 = E_{S,0}^X/\hbar$ to be approximately constant, the amplitude coefficients of the exciton states is written as $\tilde{c}_{S,\mathbf{Q}}^{(1)}(t) \approx \tilde{\gamma}_0(t) \frac{\tilde{M}_{S,\mathbf{Q}}^{\hat{\mathbf{e}},\ell,p}}}{\hbar\omega_0}$, where $\tilde{\gamma}_{S,\mathbf{Q}}(t) \approx \tilde{\gamma}_0(t) \equiv \tilde{\gamma}_0(t)$. Thus the envelope function of SFME state for the S band excited by the $\hat{\mathbf{e}}$ -polarized TL in the (ℓ, p) -mode can be written as $\tilde{F}_S^{\hat{\mathbf{e}},\ell,p}(\mathbf{R}_c, t) \approx \tilde{\gamma}_0(t) \tilde{f}_S^{\hat{\mathbf{e}},\ell,p}(\mathbf{R}_c)$ in a separable form, where $\tilde{\gamma}_0(t)$ is the factor absorbing the all time-dependencies and

$$\tilde{f}_S^{\hat{\mathbf{e}},\ell,p}(\mathbf{R}_c) = \frac{1}{\hbar\omega_0} \frac{1}{\sqrt{\Omega}} \sum_{\mathbf{Q}} \tilde{M}_{S,\mathbf{Q}}^{\hat{\mathbf{e}},\ell,p} e^{i\mathbf{Q}\cdot\mathbf{R}_c}, \quad (12)$$

is defined to describe the static part of the envelope function, where the optical matrix element, $\tilde{M}_{S,\mathbf{Q}}^{\hat{\mathbf{e}},\ell,p}$, is acting as the co-

efficient of the Fourier transform component of the envelope function, $\tilde{f}_S^{\hat{\mathbf{e}},\ell,p}(\mathbf{R}_c)$, of the TL-induced SFME state in the center-of-mass coordinate \mathbf{R}_c -space. Thus the contour pattern of $\tilde{M}_{S,\mathbf{Q}}^{\hat{\mathbf{e}},\ell,p}$ over the \mathbf{Q} -space for the SFME state excited by $\hat{\mathbf{e}}$ -polarized TL in the (ℓ, p) mode directly maps out the finite-momentum exciton components therein, from which one can further infer the shape of the SFME state in the real space described by $\tilde{f}_S^{\hat{\mathbf{e}},\ell,p}(\mathbf{R}_c)$. In other words, a TL-induced SFME state can be re-shaped by switching the (ℓ, p) mode of the LG beam or directly changing the light polarization. In fact, engineering or guiding the center-of-mass motion of an exciton is not a trivial task because of charge neutrality of exciton [25–27]. Here, we find that the application of TL provides an alternative possible route to forming and shaping the envelope function of SFME states. As suggested by Ref. [69], the decoherence coming from the exciton-exciton and exciton-phonon interactions can be suppressed by reducing the exciton density and temperature, respectively. By means of the technology, the twisted light induced SFME states in TMD-MLs might preserve the coherence and allow for optically guiding prior to the spontaneous radiative recombination happening within the subpicosecond time period.

In the remainder part of this work, we will investigate how to tailor the geometric shape of the envelope function of the SFME state in TMD-ML's using polarized TL and analyze the ℓ - and p -dependent optical matrix elements of the TL-tailored SFME states.

III. RESULTS AND DISCUSSIONS

A. Formation of SFME states by TL

1. Optical matrix elements of excitons and the reciprocal amplitude functions of LG TL

First, we consider the exciton states photogenerated by normally incident polarized LG beams in the fundamental mode $(\ell, p) = (0, 0)$. Figures 3(c) and 3(e) show the square of magnitude of the optical matrix elements, $|\tilde{M}_{S=\pm,\mathbf{Q}}^{\hat{\sigma}^+,0,0}|^2$, for the \mathbf{Q} -exciton components in the upper and lower exciton band, respectively, excited by a circularly $\hat{\sigma}^+$ -polarized fundamental (0,0)-LG beam.

From Eq. (10), one realizes that the complex optical matrix elements, $\tilde{M}_{S,\mathbf{Q}}^{\hat{\mathbf{e}},\ell,p}$ for the \mathbf{Q} -exciton components in a TL-generated SFME state are determined by the kind of mode of the exciting LG beam as well as the polarization $\hat{\mathbf{e}}$. This indicates that the superposition of the \mathbf{Q} -exciton components in a SFME state can be specified by the selected polarization, $\hat{\mathbf{e}}$, of incident TL. Thus, because the magnitude of the dipole-coupling term $|\hat{\sigma}^+ \cdot \mathbf{D}_{\pm,\mathbf{Q}}^{X*}| = D_0^X/\sqrt{2}$ in Eq. (10) remains constant for all the \mathbf{Q} -exciton states coupled to the circularly polarized beam, the optical matrix elements $\tilde{M}_{S,\mathbf{Q}}^{\hat{\sigma}^+,0,0}$ follows the same distribution over the \mathbf{Q} -space as that of the amplitude function $\mathcal{A}_{00}(\mathbf{Q})$ of the incident circularly polarized TL. For reference, Fig. 3(a) presents the contour-plot of the $|\mathcal{A}_{00}(\mathbf{q}_{\parallel})|^2$ of the fundamental LG beam in the \mathbf{q}_{\parallel} -space, schematically highlighted with the circular arrow lines representing the circular polarization, $\hat{\mathbf{e}} = \hat{\sigma}^+$, carried by the incident LG beam. With the beam waist of LG beam $W_0 = 1.5 \mu\text{m}$, $|\mathcal{A}_{00}(\mathbf{q}_{\parallel})|^2 \propto \exp(-q_{\parallel}^2 W_0^2/2)$ spreads over a finite \mathbf{q}_{\parallel} -area at the scale of

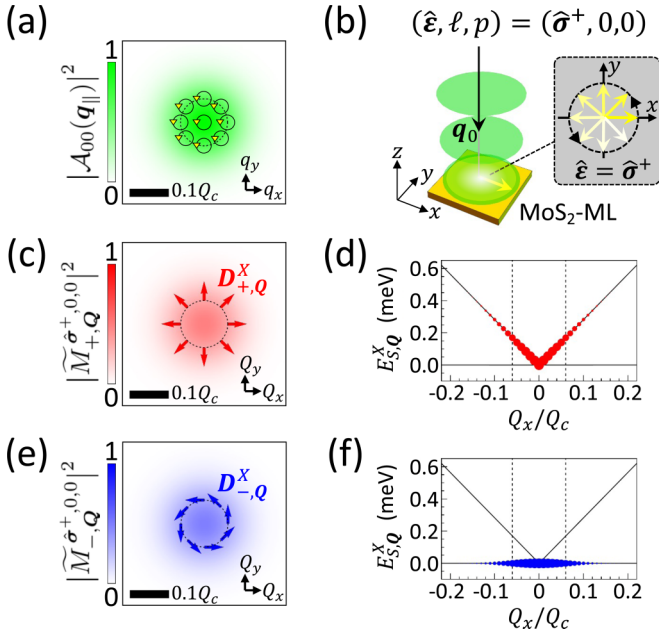


FIG. 3. (a) The square of the magnitude of the amplitude function, $|\mathcal{A}_{\ell p}(q_{\parallel})|^2$, of normally incident circularly polarized LG beam in the fundamental mode with $\mathbf{q}_0 = q_0 \hat{z}$ and $(\hat{\epsilon}, \ell, p) = (\hat{\sigma}^+, 0, 0)$, where the spiral arrow lines schematically indicate the circular polarization of TL. (b) Schematics of a MoS₂ monolayer under the photoexcitation of the circularly polarized TL. (c) The square of the magnitude of the optical matrix elements, $|\tilde{M}_{S=+,Q}^{\hat{\sigma}^+,0,0}|^2$, of the valley-mixed exciton states in the upper band, where the red arrow lines depict the longitudinal dipole moments, $\mathbf{D}_{+,Q}^X \parallel \mathbf{Q}$, of the TL-excited exciton states with $Q = 0.06Q_c$ [indicated also by the vertical dashed lines in (d) and (f)]. (d) The valley-split exciton band structure and the exciton states photogenerated by the fundamental LG TL in the upper band, marked by the red filled circles whose sizes reflect the magnitudes of $|\tilde{M}_{+,Q}^{\hat{\sigma}^+,0,0}|^2$ of the states. (e) and (f) present the results as (c) and (d), but for the exciton states in the lower band. Note the photoexcited exciton states in the lower band carrying the transverse dipole moments, $\mathbf{D}_{-,Q}^X \perp \mathbf{Q}$.

characteristic length $\sim 0.1Q_c$, so does the $|\tilde{M}_{S,Q}^{\hat{\sigma}^+,0,0}|^2$ as seen in Figs. 3(c) and 3(e).

The optical matrix elements, $\tilde{M}_{S,Q}^{\hat{\sigma}^+,0,0}$, are known from Eq. (12) to determine the amplitudes of the finite- Q exciton components in the TL-generated SFME state. The magnitudes of $\tilde{M}_{+,Q}^{\hat{\sigma}^+,0,0}$ [$\tilde{M}_{-,Q}^{\hat{\sigma}^+,0,0}$] for the SFME state formed in the upper [lower] exciton band are represented by the sizes of filled circles placed on the Q -exciton states of the upper [lower] band shown in Fig. 3(d) [Fig. 3(f)]. Figures 3(d) and 3(f) show the finite- Q exciton components in the TL-excited SFME state that are distributed over the *upward* dispersions of the exciton bands. Accordingly, one can naturally infer the spectral *blueshifts* of the SFME states under the photoexcitation of the TL in the higher-order modes, as observed by Ref. [40].

2. Shaping the envelope function of SFME states by using polarized TL

Next, we turn to consider linearly polarized LG beams and examine the resulting SFME states. Figures 4(c) and 4(e)

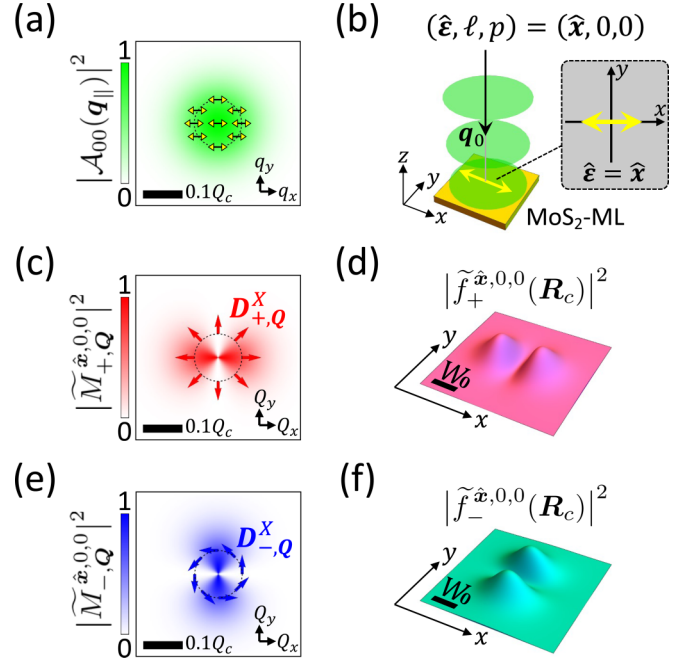


FIG. 4. (a) The square of the magnitude of the amplitude function, $|\mathcal{A}_{\ell p}(q_{\parallel})|^2$, of normally incident linearly \hat{x} -polarized LG beam in the fundamental mode, where the horizontal arrow lines indicate the linear polarization of the applied TL. (b) Schematics of a MoS₂ monolayer excited by the linearly polarized TL. (c) The square of the magnitude of the optical matrix elements in the \mathbf{Q} -space, $|\tilde{M}_{+,Q}^{\hat{x},0,0}|^2$, and (d) the envelope functions in the \mathbf{R}_c -space, $|\tilde{f}_{+,0,0}^{\hat{x}}(\mathbf{R}_c)|^2$, of the finite- Q exciton states in the upper band photoexcited by the linearly polarized fundamental LG TL, where the black bar in (d) represents the length of beam waist of the exciting TL, $W_0 = 1.5 \mu\text{m}$. (e) and (f) present the results as (c) and (d), but for the transverse exciton states excited by the same polarized TL in the lower band.

show the square of magnitude of the complex optical matrix element $|\tilde{M}_{S,Q}^{\hat{x},0,0}|^2$ over the \mathbf{Q} -space for the *linearly* \hat{x} -polarized LG beam in the fundamental (0,0)-mode. Differing from the cases of circularly polarized beam, the dipole-field coupling terms, $\hat{x} \cdot \mathbf{D}_{-,Q}^{X*} = iD_0^X \sin \phi_Q$ and $\hat{x} \cdot \mathbf{D}_{+,Q}^{X*} = D_0^X \cos \phi_Q$, in Eq. (10) arising from the linearly polarized beam are no longer constant and highly depend on the orientation of the \mathbf{Q} -vector. With the ϕ_Q dependence of the dipole-field coupling terms, the contour pattern of $|\tilde{M}_{S,Q}^{\hat{x},0,0}|^2$ over the \mathbf{Q} -space is reshaped to be highly anisotropic.

For the upper exciton band, as shown in Fig. 4(c), the \hat{x} -polarized LG beam selectively couples the exciton states with the wave vectors surrounding the Q_x axis. Correspondingly, the SFME state photogenerated by the \hat{x} -polarized LG beam for the exciton upper band is more localized along the \hat{x} direction in the real space (that is parallel to the \hat{x} polarization of the exciting beam) and nearly vanishing around the y axis in the real space, as described by $|\tilde{f}_{+,0,0}^{\hat{x}}(\mathbf{R}_c)|^2$ shown in Fig. 4(d).

By contrast, the photogenerated SFME state in the lower band by the same \hat{x} -polarized LG beam superpositions the finite momentum exciton states surrounding the Q_y axis in the \mathbf{Q} -space and the resulting SFME state turns out to be localized in the \hat{y} direction in the real space (that is perpendicular to the

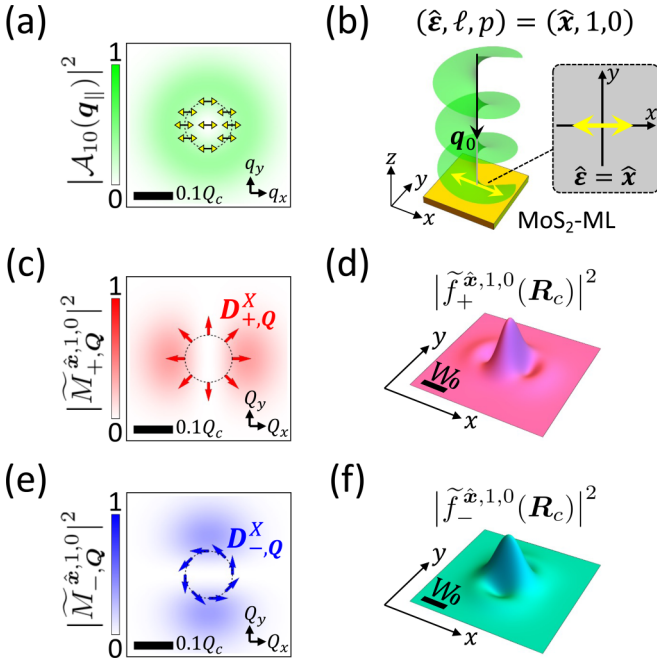


FIG. 5. (a) The square of the magnitude of the amplitude function, $|\mathcal{A}_{\ell p}(\mathbf{q}_{||})|^2$, of the high-order LG beam carrying the finite OAM, $\ell = 1$, with $\mathbf{q}_0 = q_0 \hat{z}$ and the mode indices $(\hat{\mathbf{e}}, \ell, p) = (\hat{\mathbf{x}}, 1, 0)$. (b) Schematics of a MoS₂ monolayer under the excitation of the linearly polarized TL with $(\hat{\mathbf{e}}, \ell, p) = (\hat{\mathbf{x}}, 1, 0)$. (c) The square of the magnitude of the optical matrix elements in the \mathbf{Q} -space, $|\tilde{M}_{+,Q}^{\hat{\mathbf{x}},1,0}|^2$, and (d) the envelope functions in the \mathbf{R}_c -space, $|\tilde{f}_{+, \hat{\mathbf{x}}, 1, 0}(\mathbf{R}_c)|^2$, of the finite- \mathbf{Q} exciton states in the upper band photoexcited by the $\hat{\mathbf{x}}$ -polarized TL with $\ell = 1$, where the length of the black scale bar is, $W_0 = 1.5 \mu\text{m}$, for reference. (e) and (f) present the results as (c) and (d), but for the TL-excited exciton states in the lower band.

$\hat{\mathbf{x}}$ polarization of the exciting beam), as shown in Figs. 4(e) and 4(f).

The above studies show that the SFME states optically generated in the valley-split exciton bands by a TL can be engineered by the selection of the polarization of the exciting TL. Besides, whereas the valley-mixed exciton bands split by only few meV are usually hardly resolved [21,23,40,50] and identified spectrally, the TL-excited SFME states in the upper and lower bands present the completely distinctive \mathbf{Q} distributions of the optical matrix elements, suggesting the distinct angle-dependent optical spectra of the upper- and lower-band SFME states.

3. ℓ - and p -dependent SFME states

After recognizing the shaping effect of light polarization (SAM of light) on TL-generated SFME states, we proceed with the investigation of the photoexcitations in the TMD-ML's by the TL carrying nonzero $\ell \neq 0$ (OAM of light). Figures 5(c) and 5(e) show the square of magnitudes of the \mathbf{Q} -dependent optical matrix elements $|\tilde{M}_{S=\pm, Q}^{\hat{\mathbf{x}}, 1, 0}|^2$ of the SFME states in the upper and lower exciton band excited by the normally incident $\hat{\mathbf{x}}$ -polarized LG beams in the mode of $(\ell, p) = (1, 0)$, respectively. For reference of Figs. 5(c) and 5(e), Fig. 5(a) plots the amplitude function $|\mathcal{A}_{10}(\mathbf{q}_{||})|^2$ featured

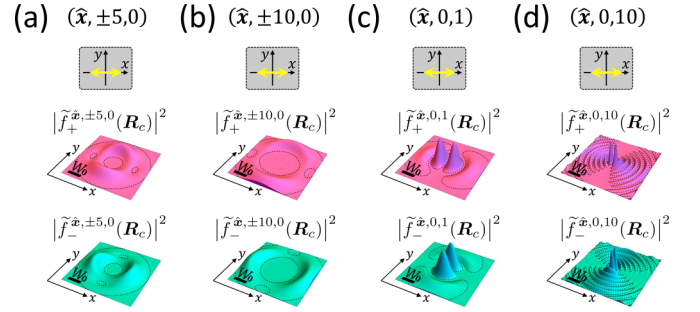


FIG. 6. The real-space envelope functions $|\tilde{f}_{S=\pm}^{\hat{\mathbf{e}}, \ell, p}(\mathbf{R}_c)|^2$ of the SFME states in a MoS₂-ML photogenerated by the higher-order $\hat{\mathbf{x}}$ -polarized LG TL with (a) $(\hat{\mathbf{e}}, \ell, p) = (\hat{\mathbf{x}}, \pm 5, 0)$, (b) $(\hat{\mathbf{e}}, \ell, p) = (\hat{\mathbf{x}}, \pm 10, 0)$, (c) $(\hat{\mathbf{e}}, \ell, p) = (\hat{\mathbf{x}}, 0, 1)$, and (d) $(\hat{\mathbf{e}}, \ell, p) = (\hat{\mathbf{x}}, 0, 10)$. The dotted contour lines in all plots have the equal value of 0.01.

with the ring-like contours in the $\mathbf{q}_{||}$ -space and highlighted with the horizontal arrow lines representing the $\hat{\mathbf{x}}$ polarization of the incident TL.

From Eqs. (10) and (12), the amplitude function of the Fourier transform of the SFME states induced by $\hat{\mathbf{x}}$ -polarized TL are given by $\tilde{M}_{S, Q}^{\hat{\mathbf{x}}, \ell, p} \propto \mathcal{A}_{\ell p}(\mathbf{Q})(\hat{\mathbf{x}} \cdot \mathbf{D}_{S, Q}^{X*})$, which are determined by the product of the amplitude function of TL, $\mathcal{A}_{\ell p}(\mathbf{Q})$, and the dipole coupling term, $(\hat{\mathbf{x}} \cdot \mathbf{D}_{S, Q}^{X*})$. Accordingly, we obtain $\tilde{M}_{+, Q}^{\hat{\mathbf{x}}, \ell, p} \propto \mathcal{A}_{\ell p}(\mathbf{Q}) \cos \phi_Q$ and $\tilde{M}_{-, Q}^{\hat{\mathbf{x}}, \ell, p} \propto \mathcal{A}_{\ell p}(\mathbf{Q}) \sin \phi_Q$. It turns out that, in Figs. 5(c) [5(e)], the square of magnitude of the optical matrix elements of the upper [lower] exciton band, $\tilde{M}_{+, Q}^{\hat{\mathbf{x}}, \ell, 0}$ [$\tilde{M}_{-, Q}^{\hat{\mathbf{x}}, \ell, 0}$] for $|\ell| = 1$ becomes highly anisotropic and distributed mainly around the positive and negative Q_x axes [Q_y axis] in the \mathbf{Q} -plane.

Correspondingly, Figs. 5(d) and 5(f) show the square of magnitude of the real-space envelope functions $|\tilde{f}_{S=\pm}^{\hat{\mathbf{x}}, 1, 0}(\mathbf{R}_c)|^2$ of the SFME states photogenerated in the upper and lower exciton band, respectively, by the incident of (1,0) LG TL. As compared with the semi-ring-like SFME states excited by the fundamental LG beam with the nodes at the origin $\mathbf{R}_c = \mathbf{0}$ [see Figs. 4(d) and 4(f)], the SFME states excited by the LG beam with $\ell = 1$ shown in Figs. 5(d) and 5(f) are nodeless at the origin position. According to Eq. (12), the envelope function of a SFME state at the origin $\mathbf{R}_c = \mathbf{0}$ is given by $\tilde{f}_{\pm}^{\hat{\mathbf{x}}, \ell, p}(\mathbf{R}_c = \mathbf{0}) \propto \int d^2\mathbf{Q} \tilde{M}_{\pm, Q}^{\hat{\mathbf{x}}, \ell, p}$. Following Eq. (10), one can show that $\tilde{M}_{\pm, Q}^{\hat{\mathbf{x}}, \ell, p} \propto e^{i\ell\phi_Q}(e^{i\phi_Q} \pm e^{-i\phi_Q})$, where the term $e^{i\ell\phi_Q}$ is arising from $\mathcal{A}_{\ell p}(\mathbf{Q})$ and the one $(e^{i\phi_Q} \pm e^{-i\phi_Q})$ is from the dipole coupling term, $(\hat{\mathbf{x}} \cdot \mathbf{D}_{\pm, Q}^{X*})$, of Eq. (10). Thus one can derive that $\tilde{f}_{\pm}^{\hat{\mathbf{x}}, \ell, p}(\mathbf{R}_c = \mathbf{0}) \propto \int_0^{2\pi} d\phi_Q e^{i\ell\phi_Q}(e^{i\phi_Q} \pm e^{-i\phi_Q}) \propto (\delta_{\ell, -1} \pm \delta_{\ell, 1})$. This shows that, under the linearly polarized TL excitation, the TL-excited SFME states normally should have the nodes at $\mathbf{R}_c = \mathbf{0}$, unless the exciting TL carrying the OAM's, $\ell = \pm 1$. The exceptional hut-like envelop functions nodeless at the origin results from the cancellation of the phase winding numbers, $n_w^{\ell} = \pm 1$, of optical OAM $\ell = \pm 1$ and those of the \mathbf{Q} -dependent dipoles of valley exciton, $n_w^X = \mp 1$, and manifest the interplay between the optical OAM and dipolar valley exciton.

Further, let us examine the effects of the LG TL with higher ℓ 's. Figures 6(a) and 6(b) show that the real-space SFME

states of the upper (lower) band photoexcited by the high- ℓ LG TL are split into the shape of saddle featured with the nodes at $\mathbf{R}_c = \mathbf{0}$ and elongated along the positive and negative y semiaxis (x semiaxis), consistent with the predicted nodes at $\mathbf{R}_c = \mathbf{0}$ for $\ell \neq \pm 1$ by our previous analysis. To see a more thorough analysis including the study of \mathbf{Q} -dependent optical matrix elements, please refer to Ref. [43].

Besides the OAM's, the spatial structures of LG TL are characterized also by the radial indices, p . Figs 6(c) and 6(d) show the envelope functions, $|\tilde{f}_{\pm}^{\hat{x},0,p}(\mathbf{R}_c)|^2$, in real space resulting from the photoexcitations of normally incident \hat{x} -polarized LG beams with $\ell = 0$ and $p = 1$ and 10. One notes that the real-space envelop functions of the SFME states excited by the LG TL with $p \neq 0$ exhibit very different patterns from those excited by OAM TL with $p = 0$ shown by Figs. 4, 5 and 6(a), 6(b). Inheriting from the multiple-ring patterns of the amplitude function $|\mathcal{A}_{0p}(\mathbf{Q})|^2$ of the high order LG TL with $p \neq 0$ (see Fig. S3 in Ref. [43]), the rippling features are also retained in the real-space envelope functions of the SFME states, as shown by the plots of $|\tilde{f}_{\pm}^{\hat{x},0,p}(\mathbf{R}_c)|^2$ in Figs. 6(c) and 6(d).

In general, the optical OAM is actually transferrable to the both center-of-mass motion as well as the relative e - h motion of exciton, as justified by the group-theory study of Ref. [70]. In this work, we show that the OAM carried by a twisted light affects only the CoM motion of the lowest 1s exciton since the lowest 1s exciton states carries no internal angular momentum. The interaction between twisted light and high lying exciton states with nonzero internal angular momenta and the resulting new optical selection rules for the internal angular momentum of exciton are certainly crucial and worthy of studying in the future.

B. Momentum-dependent optical matrix elements (MD-OME's)

The formation of the SFME states should make impacts on the optical properties of a TMD-ML under the excitation of TL. While many optical processes in materials involve complex relaxation and dephasing mechanisms that are beyond the scope of this work, in this section we shall examine the optical matrix elements (OME's) with respect to the SFME states of a TL-excited TMD-ML, which offer fundamental parameters for further sophisticate simulation of the realistic optical processes, e.g., photoluminescence or absorption [71]. In the angular spectrum representation, one is concerned with the momentum-dependent OME regarding a plane-wave of light with the wave vector \mathbf{q} . The square magnitude of OME determines the rate of optical transition from an exciton state and \mathbf{q} dependence of OME manifests the angle dependence of optical spectrum.

The OME with respect to the SFME state of a TL-excited TMD-ML is defined as $\tilde{M}_{\text{SFME}}^{\lambda,q} \equiv \langle \Psi^X(t) | \hat{H}_I^{\lambda,q}(\mathbf{r}) | GS \rangle$, where $|\Psi^X\rangle$ is the SFME state given by Eq. (9), $\hat{H}_I^{\lambda,q}(\mathbf{r})$ is the second quantized operator of the light-matter interaction for the plane-wave light with wave vector $\mathbf{q} = q_v(\sin \theta_v \cos \phi_v \hat{x} + \sin \theta_v \sin \phi_v \hat{y} + \cos \theta_v \hat{z})$ given by $\hat{H}_I^{\lambda,q}(\mathbf{r}) = \frac{|e|}{2m_0} \mathbf{A}_q^{\hat{x},q}(\mathbf{r}) \cdot \mathbf{p}$, θ_v (ϕ_v) is the polar (azimuthal) angle of the light wave vector, $\mathbf{A}_q^{\hat{x},q}(\mathbf{r}) = \hat{\mathbf{e}}_{\lambda,q} A_0 e^{i\mathbf{q}\cdot\mathbf{r}}$ is the vector potential of the plane-wave, and $\hat{\mathbf{e}}_{\lambda=1,q} = \cos \theta_v (\cos \phi_v \hat{x} + \sin \phi_v \hat{y}) - \sin \theta_v \hat{z}$ and

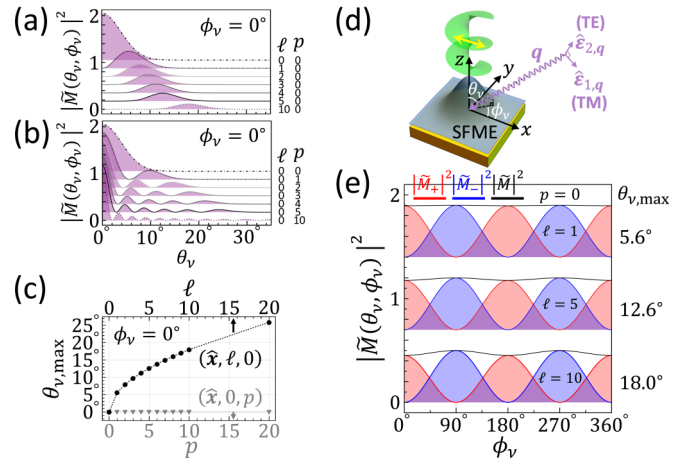


FIG. 7. The θ_v -dependent OME's, $|\tilde{M}(\theta_v, \phi_v = 0^\circ)|^2$, of the SFME states in a MoS₂ monolayer along the fixed x - z plane ($\phi_v = 0^\circ$) and with varied polar angles (θ_v), photogenerated by the \hat{x} -polarized TL with (a) ($\hat{\mathbf{e}} = \hat{\mathbf{x}}$, $\ell = 0, 1, \dots, 5, 10$, $p = 0$) and (b) ($\hat{\mathbf{e}} = \hat{\mathbf{x}}$, $\ell = 0, p = 0, 1, \dots, 5, 10$). From (a) and (b), (c) records the polar angles, $\theta_{v,\text{max}}$, of the maximum magnitude of the MD-OME of the SFME states photogenerated by the TL in the various modes of $(\ell, 0)$ and $(0, p)$. The obvious ℓ dependence of $\theta_{v,\text{max}}$ indicates the OAM-encoded polar angles in the MD-OME's of the TL-excited SFME states. (d) Schematics illustrating the polar, θ_v , and azimuthal angle, ϕ_v , of a coupled plane-wave light with wave vector \mathbf{q} considered in the MD-OME simulation. (e) The ϕ_v dependence of $|\tilde{M}_{S=\pm}(\theta_{v,\text{max}}, \phi_v)|^2$ for the SFME states formed in the upper ($S = +$) and lower ($S = -$) exciton bands excited by the normal incident TL with ($\hat{\mathbf{e}} = \hat{\mathbf{x}}$, $\ell = 1, 5, 10$, $p = 0$) at $\theta_v = \theta_{v,\text{max}}$. One notes that $|\tilde{M}_+|^2$ and $|\tilde{M}_-|^2$ follow the distinct and complementary ϕ_v -dependencies, allowing for selectively detecting the optical signals from the valley-split exciton bands according to the azimuthal angles.

$\hat{\mathbf{e}}_{\lambda=2,q} = -\sin \phi_v \hat{x} + \cos \phi_v \hat{y}$ are the polarization basis of TM and TE mode of light, respectively [see the schematics plotted in Fig. 7(d)]. Since optical transitions could only be significantly triggered by the light with energy resonant to the SFME state, we define the momentum-dependent (MD) OME of a SFME state, $|\tilde{M}(\theta_v, \phi_v)|^2 \equiv \sum_{\lambda=1}^2 |\tilde{M}_{\text{SFME}}^{\lambda,q_c}|^2 = |\tilde{M}_+(\theta_v, \phi_v)|^2 + |\tilde{M}_-(\theta_v, \phi_v)|^2$, with respect to the TM ($\lambda = 1$) and TE ($\lambda = 2$) light with energy equal to the exciton band edge, $E_{S,0}^X = \hbar c Q_c$, where $\mathbf{q}_c = Q_c(\sin \theta_v \cos \phi_v \hat{x} + \sin \theta_v \sin \phi_v \hat{y} + \cos \theta_v \hat{z})$ is the wave vector of the resonant light. $|\tilde{M}_{+/-}(\theta_v, \phi_v)|^2$ is the OME contributed by the upper/lower ($S = +/-$) exciton band components in the SFME state given by Eq. (9). For the SFME states generated by the \hat{x} -polarized TL with ℓ and p degrees of freedom, we can follow the definition of $\tilde{M}_{\text{SFME}}^{\lambda,q_c}$ and neglect the dispersion of exciton states ($\omega_{S,Q} \approx \omega_0$) to evaluate the MD-OME as

$$|\tilde{M}(\theta_v, \phi_v)|^2 \propto |\tilde{M}_{+,q_{c,\parallel}}^{\hat{x},\ell,p}|^2 \cos^2 \theta_v + |\tilde{M}_{-,q_{c,\parallel}}^{\hat{x},\ell,p}|^2, \quad (13)$$

where $q_{c,\parallel}$ is the in-plane component of $\mathbf{q}_c = \mathbf{q}_{c,\parallel} + Q_c \cos \theta_v \hat{z}$. The appearance of $\cos^2 \theta_v$ in the first term on the right-hand side of Eq. (13) arises from the partial projection of the polarization of TM light onto the longitudinal dipoles of

the upper-band exciton states, $|\hat{\mathbf{e}}_{\lambda=1, q_c} \cdot \mathbf{D}_{S=+, q_c, \parallel}^{X*}|^2 \propto \cos^2 \theta_v$ (similar arguments for the absorption spectra in MoS₂-ML's could be found in Ref. [21]).

From Eq. (13), one can note that the angle dependence of $|\tilde{M}(\theta_v, \phi_v)|^2$ is correlated to the $\mathbf{q}_{c, \parallel}$ distribution of the square of the magnitude of the optical matrix elements, $|\tilde{M}_{\pm, \mathbf{q}=\mathbf{q}_{c, \parallel}}^{\hat{\mathbf{x}}, \ell, p}|^2$. Taking the relation of $\tilde{M}_{\pm, \mathbf{q}_{c, \parallel}}^{\hat{\mathbf{x}}, \ell, p} \propto \mathcal{A}_{\ell p}(\mathbf{q}_{c, \parallel})(\hat{\mathbf{x}} \cdot \mathbf{D}_{\pm, \mathbf{q}_{c, \parallel}}^{X*})$ from Eq. (10), the MD-OME from a TL-induced SFME state in Eq. (13) composed of the contributions from the upper and lower exciton bands reads, $|\tilde{M}(\theta_v, \phi_v)|^2 \propto |\mathcal{A}_{\ell p}(\mathbf{q}_{c, \parallel})|^2 \cos^2 \phi_v \cos^2 \theta_v + |\mathcal{A}_{\ell p}(\mathbf{q}_{c, \parallel})|^2 \sin^2 \phi_v$.

Accordingly, Figs. 7(a) and 7(b) show the θ_v dependence of the MD-OME, $|\tilde{M}(\theta_v, 0)|^2$, in the x - z plane ($\phi_v = 0$) from the SFME states in a TMD-ML photoexcited by the TL with $\{\ell = 0, 1, 2, \dots, p = 0\}$ and $\{\ell = 0, p = 0, 1, 2, \dots\}$, respectively. Since $|\tilde{M}_-(\theta_v, \phi_v = 0)|^2 \propto \sin^2(\phi_v = 0) = 0$, the MD-OME in the x - z plane is solely from the upper exciton band, $|\tilde{M}(\theta_v, 0)|^2 = |\tilde{M}_+(\theta_v, 0)|^2 \propto |\mathcal{A}_{\ell p}(\mathbf{q}_{c, \parallel})|^2 \cos^2 \theta_v$. Hence, with increasing ℓ , the direction of the MD-OME with maximum value is tilted from the z -axis with increasing $\theta_v \equiv \theta_{v, \max}$ as shown in Fig. 7(a), following the similar q_x dependence to that of $|\mathcal{A}_{\ell p}(\mathbf{q}_{c, \parallel})|^2$ (see Fig. S2(a) in Ref. [43]). By contrast, as shown in Fig. 7(b), the MD-OME with the maximum value remains at $\theta_v = 0$ with fixed $\ell = 0$ and increasing $p = 0, 1, 2, \dots$, consistent with the q_x dependencies of $|\mathcal{A}_{\ell p}(\mathbf{q}_{c, \parallel})|^2$ (see Fig. S3(a) in Ref. [43]). Figure 7(c) shows how the polar angle, $\theta_{v, \max}$, of the MD-OME with maximum value of the TL-excited SFME states depend on the OAM's (filled circles) and the radial indices (filled triangles) of the exciting TL with $(\ell, p = 0)$ and $(\ell = 0, p)$, respectively. Apparently, the former shows the better angle-resolved spectra for varying ℓ .

Finally, let us examine the ϕ_v dependencies of the MD-OME's from SFME states in TMD-ML's excited by LG TL. Figure 7(e) shows the magnitude square of the MD-OME's from the SFME states in the upper and lower exciton bands excited by the TL with OAM's, $\ell = 1, 5$, and 10, over the full azimuthal angular range $\phi_v = \{0^\circ, 360^\circ\}$ with the fixed $\theta_v = \theta_{v, \max}$. One notes that, under the $\hat{\mathbf{x}}$ -polarized TL excitation, the MD-OME from the upper and lower exciton bands exhibit the distinctive and complementary ϕ_v dependencies. As one sees in Fig. 7(e), the magnitude square of the MD-OME from the upper-band SFME state oscillates with ϕ_v , featured with the maximum value at the angles $\phi_v = 0^\circ, 180^\circ$, i.e., along the positive and negative x axis in *parallel*

to the $\hat{\mathbf{x}}$ polarization of the exciting TL. By contrast, the MD-OME's from the lower-band SFME states show the maximum value at the angles $\phi_v = 90^\circ, 270^\circ$, i.e., along the positive and negative y axis *perpendicular* to the $\hat{\mathbf{x}}$ polarization of the incident TL. As a main finding of this work, we show that the MD-OME of specific valley-mixed exciton bands of TMD-ML's under polarized TL are highly directional and dependent on the direction of the polarization of the applied TL. While the meV-split upper and lower exciton bands of a TMD-ML are normally hardly resolved spectrally, the MD-OME's of the SFME states under the linearly polarized TL excitation is shown to mimic an exciton multiplexer allowing for selectively detecting the optical signatures of the meV-split longitudinal and transverse exciton bands of TMD-ML's [72,73].

IV. CONCLUSIONS

In conclusion, we present a comprehensive theoretical investigation of the photogenerated valley excitons in TMD-ML's by Laguerre-Gaussian (LG) beams, one of the best known twisted light carrying optical OAM, in addition to optical SAM. We show that a normally incident polarized LG beam to a TMD-ML photogenerates the SAM- and OAM-encoded superposition of finite-momentum exciton (SFME) states, whose distributions over the exciton-momentum space are determined by the intriguing interplay between multiple photonic and excitonic degrees of freedom, including the OAM and SAM of light, and the valley pseudospin and center-of-mass motion of exciton. This reveals the possibilities of using polarized TL with engineered OAM to optically localize, shape and guide the finite momentum exciton states, a key feature desired by the advanced optoelectronic applications and fundamental research that require charge-neutral excitons to be transported. The spatial structures of exciting TL are shown directly to impact the momentum-dependent optical matrix elements of the TL-generated SFME states, which manifest the angle-dependent optical properties of TL-excited TMD-ML's.

ACKNOWLEDGMENTS

This study is supported by the Ministry of Science and Technology, Taiwan, under contracts, MOST 109-2112-M-009 -018 -MY3, and by National Center for High-Performance Computing (NCHC), Taiwan. The authors are grateful to Ting-Hua Lu, Yann-Wen Lan, and Shao-Yu Chen for fruitful discussions.

-
- [1] M. Amani, D.-H. Lien, D. Kiriya, J. Xiao, A. Azcatl, J. Noh, S. R. Madhupathy, R. Addou, K. Santosh, M. Dubey *et al.*, *Science* **350**, 1065 (2015).
- [2] J. R. Schaibley, H. Yu, G. Clark, P. Rivera, J. S. Ross, K. L. Seyler, W. Yao, and X. Xu, *Nat. Rev. Mater.* **1**, 16055 (2016).
- [3] T. Mueller and E. Malic, *npj 2D Mater. Appl.* **2**, 29 (2018).
- [4] G. Wang, A. Chernikov, M. M. Glazov, T. F. Heinz, X. Marie, T. Amand, and B. Urbaszek, *Rev. Mod. Phys.* **90**, 021001 (2018).
- [5] A. Chernikov, T. C. Berkelbach, H. M. Hill, A. Rigosi, Y. Li, B. Aslan, D. R. Reichman, M. S. Hybertsen, and T. F. Heinz, *Phys. Rev. Lett.* **113**, 076802 (2014).
- [6] K. He, N. Kumar, L. Zhao, Z. Wang, K. F. Mak, H. Zhao, and J. Shan, *Phys. Rev. Lett.* **113**, 026803 (2014).
- [7] N. Lundt, S. Klemmt, E. Cherotchenko, S. Betzold, O. Iff, A. V. Nalitov, M. Klaas, C. P. Dietrich, A. V. Kavokin, S. Höfling *et al.*, *Nat. Commun.* **7**, 13328 (2016).

- [8] L. Zhang, R. Gogna, W. Burg, E. Tutuc, and H. Deng, *Nat. Commun.* **9**, 713 (2018).
- [9] Z. Wang, D. A. Rhodes, K. Watanabe, T. Taniguchi, J. C. Hone, J. Shan, and K. F. Mak, *Nature* **574**, 76 (2019).
- [10] D. Kozawa, A. Carvalho, I. Verzhbitskiy, F. Giustiniano, Y. Miyauchi, S. Mouri, A. Castro Neto, K. Matsuda, and G. Eda, *Nano Lett.* **16**, 4087 (2016).
- [11] L. Wu, Y. Chen, H. Zhou, and H. Zhu, *ACS Nano* **13**, 2341 (2019).
- [12] M. Bernardi, M. Palumbo, and J. C. Grossman, *Nano Lett.* **13**, 3664 (2013).
- [13] M.-L. Tsai, S.-H. Su, J.-K. Chang, D.-S. Tsai, C.-H. Chen, C.-I. Wu, L.-J. Li, L.-J. Chen, and J.-H. He, *ACS Nano* **8**, 8317 (2014).
- [14] S.-Y. Chen, T. Goldstein, T. Taniguchi, K. Watanabe, and J. Yan, *Nat. Commun.* **9**, 3717 (2018).
- [15] E. Liu, J. van Baren, C.-T. Liang, T. Taniguchi, K. Watanabe, N. M. Gabor, Y.-C. Chang, and C. H. Lui, *Phys. Rev. Lett.* **124**, 196802 (2020).
- [16] X.-X. Zhang, T. Cao, Z. Lu, Y.-C. Lin, F. Zhang, Y. Wang, Z. Li, J. C. Hone, J. A. Robinson, D. Smirnov *et al.*, *Nat. Nanotechnol.* **12**, 883 (2017).
- [17] M. R. Molas, C. Faugeras, A. O. Slobodeniuk, K. Nogajewski, M. Bartos, D. Basko, and M. Potemski, *2D Mater.* **4**, 021003 (2017).
- [18] G. Wang, C. Robert, M. M. Glazov, F. Cadiz, E. Courtade, T. Amand, D. Lagarde, T. Taniguchi, K. Watanabe, B. Urbaszek *et al.*, *Phys. Rev. Lett.* **119**, 047401 (2017).
- [19] Z. Li, T. Wang, C. Jin, Z. Lu, Z. Lian, Y. Meng, M. Blei, M. Gao, T. Taniguchi, K. Watanabe *et al.*, *ACS Nano* **13**, 14107 (2019).
- [20] M. He, P. Rivera, D. Van Tuan, N. P. Wilson, M. Yang, T. Taniguchi, K. Watanabe, J. Yan, D. G. Mandrus, H. Yu *et al.*, *Nat. Commun.* **11**, 1 (2020).
- [21] D. Y. Qiu, T. Cao, and S. G. Louie, *Phys. Rev. Lett.* **115**, 176801 (2015).
- [22] S. Brem, A. Ekman, D. Christiansen, F. Katsch, M. Selig, C. Robert, X. Marie, B. Urbaszek, A. Knorr, and E. Malic, *Nano Lett.* **20**, 2849 (2020).
- [23] G.-H. Peng, P.-Y. Lo, W.-H. Li, Y.-C. Huang, Y.-H. Chen, C.-H. Lee, C.-K. Yang, and S.-J. Cheng, *Nano Lett.* **19**, 2299 (2019).
- [24] P.-Y. Lo, G.-H. Peng, W.-H. Li, Y. Yang, and S.-J. Cheng, *Phys. Rev. Res.* **3**, 043198 (2021).
- [25] M. Onga, Y. Zhang, T. Ideue, and Y. Iwasa, *Nat. Mater.* **16**, 1193 (2017).
- [26] X.-C. Yang, H. Yu, and W. Yao, *Phys. Rev. B* **104**, 245305 (2021).
- [27] F. Fedichkin, T. Guillet, P. Valvin, B. Jouault, C. Brimont, T. Bretagnon, L. Lahourcade, N. Grandjean, P. Lefebvre, and M. Vladimirova, *Phys. Rev. Appl.* **6**, 014011 (2016).
- [28] L. Allen, M. W. Beijersbergen, R. J. C. Spreeuw, and J. P. Woerdman, *Phys. Rev. A* **45**, 8185 (1992).
- [29] H. He, M. E. J. Friese, N. R. Heckenberg, and H. Rubinsztein-Dunlop, *Phys. Rev. Lett.* **75**, 826 (1995).
- [30] Y. Shen, X. Wang, Z. Xie, C. Min, X. Fu, Q. Liu, M. Gong, and X. Yuan, *Light Sci. Appl.* **8**, 90 (2019).
- [31] K. Y. Bliokh and F. Nori, *Phys. Rep.* **592**, 1 (2015).
- [32] M. Erhard, R. Fickler, M. Krenn, and A. Zeilinger, *Light Sci. Appl.* **7**, 17146 (2018).
- [33] A. E. Willner, K. Pang, H. Song, K. Zou, and H. Zhou, *Appl. Phys. Rev.* **8**, 041312 (2021).
- [34] A. Sit, F. Bouchard, R. Fickler, J. Gagnon-Bischoff, H. Larocque, K. Heshami, D. Elser, C. Peuntinger, K. Günthner, B. Heim *et al.*, *Optica* **4**, 1006 (2017).
- [35] M. Padgett and R. Bowman, *Nat. Photonics* **5**, 343 (2011).
- [36] G. F. Quinteiro, D. E. Reiter, and T. Kuhn, *Phys. Rev. A* **91**, 033808 (2015).
- [37] Y. Kozawa, D. Matsunaga, and S. Sato, *Optica* **5**, 86 (2018).
- [38] Y. Ueno, Y. Toda, S. Adachi, R. Morita, and T. Tawara, *Opt. Express* **17**, 20567 (2009).
- [39] K. Shigematsu, K. Yamane, R. Morita, and Y. Toda, *Phys. Rev. B* **93**, 045205 (2016).
- [40] K. B. Simbulan, T.-D. Huang, G.-H. Peng, F. Li, O. J. Gomez Sanchez, J.-D. Lin, C.-I. Lu, C.-S. Yang, J. Qi, S.-J. Cheng *et al.*, *ACS Nano* **15**, 3481 (2021).
- [41] D. Y. Qiu, G. Cohen, D. Novichkova, and S. Refaely-Abramson, *Nano Lett.* **21**, 7644 (2021).
- [42] G. Kresse and J. Furthmüller, *Phys. Rev. B* **54**, 11169 (1996).
- [43] See Supplemental Material <http://link.aps.org/supplemental/10.1103/PhysRevB.106.155304> for technical information about how to establish the Bethe-Salpeter equation on the first-principles base, evaluate the transition dipole of an exciton, and parametrize the pseudospin model for valley exciton, and the formalisms of Laguerre Gaussian beams and exciton wave packets.
- [44] J. P. Perdew, K. Burke, and M. Ernzerhof, *Phys. Rev. Lett.* **77**, 3865 (1996).
- [45] J. Heyd, G. E. Scuseria, and M. Ernzerhof, *J. Chem. Phys.* **118**, 8207 (2003).
- [46] J. Heyd and G. E. Scuseria, *J. Chem. Phys.* **121**, 1187 (2004).
- [47] A. V. Krukau, O. A. Vydrov, A. F. Izmaylov, and G. E. Scuseria, *J. Chem. Phys.* **125**, 224106 (2006).
- [48] K. F. Mak, K. He, C. Lee, G. H. Lee, J. Hone, T. F. Heinz, and J. Shan, *Nat. Mater.* **12**, 207 (2013).
- [49] D. Y. Qiu, F. H. da Jornada, and S. G. Louie, *Phys. Rev. Lett.* **115**, 119901(E) (2015).
- [50] H. Yu, G.-B. Liu, P. Gong, X. Xu, and W. Yao, *Nat. Commun.* **5**, 1 (2014).
- [51] S. Latini, T. Olsen, and K. S. Thygesen, *Phys. Rev. B* **92**, 245123 (2015).
- [52] J. P. Echeverry, B. Urbaszek, T. Amand, X. Marie, and I. C. Gerber, *Phys. Rev. B* **93**, 121107(R) (2016).
- [53] F. Fuchs, C. Rödl, A. Schleife, and F. Bechstedt, *Phys. Rev. B* **78**, 085103 (2008).
- [54] T. C. Berkelbach, M. S. Hybertsen, and D. R. Reichman, *Phys. Rev. B* **92**, 085413 (2015).
- [55] T.-i. Shibuya and C. E. Wulfman, *Am. J. Phys.* **33**, 570 (1965).
- [56] D. Parfitt and M. Portnoi, *J. Math. Phys.* **43**, 4681 (2002).
- [57] W. Hanke and L. J. Sham, *Phys. Rev. B* **12**, 4501 (1975).
- [58] L. J. Sham and T. M. Rice, *Phys. Rev.* **144**, 708 (1966).
- [59] A. A. Mostofi, J. R. Yates, G. Pizzi, Y.-S. Lee, I. Souza, D. Vanderbilt, and N. Marzari, *Comput. Phys. Commun.* **185**, 2309 (2014).
- [60] T. G. Pedersen, K. Pedersen, and T. B. Kristensen, *Phys. Rev. B* **63**, 201101(R) (2001).
- [61] R. Inoue, N. Kanai, T. Yonehara, Y. Miyamoto, M. Koashi, and M. Kozuma, *Phys. Rev. A* **74**, 053809 (2006).

- [62] F. Araoka, T. Verbiest, K. Clays, and A. Persoons, *Phys. Rev. A* **71**, 055401 (2005).
- [63] W. Löffler, D. J. Broer, and J. P. Woerdman, *Phys. Rev. A* **83**, 065801 (2011).
- [64] N. B. Clayburn, J. L. McCarter, J. M. Dreiling, M. Poelker, D. M. Ryan, and T. J. Gay, *Phys. Rev. B* **87**, 035204 (2013).
- [65] L. D. Romero, D. Andrews, and M. Babiker, *J. Opt. B* **4**, S66 (2002).
- [66] G. C. Sherman, in *Proceedings of SPIE 0358, Applications of Mathematics in Modern Optics*, edited by W. H. Carter (SPIE, 1982), Vol. 0358, pp. 31–38.
- [67] G. B. Arfken, H. J. Weber, and F. E. Harris, *Mathematical Methods for Physicists: A Comprehensive Guide* (Academic Press, 2012).
- [68] A. A. Peshkov, D. Seipt, A. Surzhykov, and S. Fritzsche, *Phys. Rev. A* **96**, 023407 (2017).
- [69] G. Moody, C. Kavir Dass, K. Hao, C.-H. Chen, L.-J. Li, A. Singh, K. Tran, G. Clark, X. Xu, G. Berghäuser *et al.*, *Nat. Commun.* **6**, 8315 (2015).
- [70] A. M. Konzelmann, S. O. Krüger, and H. Giessen, *Phys. Rev. B* **100**, 115308 (2019).
- [71] M. Selig, G. Berghäuser, M. Richter, R. Bratschitsch, A. Knorr, and E. Malic, *2D Mater.* **5**, 035017 (2018).
- [72] S. Lazić, A. Violante, K. Cohen, R. Hey, R. Rapaport, and P. V. Santos, *Phys. Rev. B* **89**, 085313 (2014).
- [73] S. Katznelson, B. Cohn, S. Sufirin, T. Amit, S. Mukherjee, V. Kleiner, P. Mohapatra, A. Patsha, A. Ismach, S. Refaely-Abramson *et al.*, *Mater. Horiz.* **9**, 1089 (2022).